THE ASTROPHYSICAL JOURNAL, 515:337–350, 1999 April 10

MULTICOMPONENT X-RAY EMISSIONS FROM REGIONS NEAR OR ON THE PULSAR SURFACE

K. S. CHENG[1] AND L. ZHANG[1,2]

Received 1998 July 30; accepted 1998 November 6

ABSTRACT

We present a model of X-ray emission from rotation-powered pulsars, which in general consist of one nonthermal component, two hard thermal components, and one soft thermal component. The nonthermal X-rays come from synchrotron radiation of $e^{\pm}$ pairs created in the strong magnetic field near the neutron star surface by curvature photons emitted by charged particles on their way from the outer gap to the neutron star surface. The first hard thermal X-ray component results from polar-cap heating by the return current in the polar gap. The second hard thermal X-ray component results from polar-cap heating by the return particles from the outer gap. Because of cyclotron resonance scattering, most of the hard thermal X-rays will be effectively reflected back to the stellar surface and eventually reemitted as soft thermal X-rays. However, some of the hard thermal X-rays can still escape along the open magnetic field lines, where the e^{+}/e^{-} pair density is low. Furthermore, the characteristic blackbody temperatures of the two hard X-ray components emitted from the polar-cap area inside the polar gap and the polar-cap area defined by the footprints of the outer-gap magnetic field lines are strongly affected by the surface magnetic field, which can be much larger than the dipolar field. In fact, the strong surface magnetic field can explain why the effective blackbody radiation area is nearly 2 orders of magnitude larger than that deduced from the dipolar field for young pulsars (2 orders of magnitude less for old pulsars). Our model indicates how several possible X-ray components may be observed, depending on the magnetic inclination angle and viewing angle. Using the expected X-ray luminosity and spectra, we explain the observed X-ray spectra from pulsars such as Geminga, PSR B1055−52, PSR B0656+14, and PSR B1929+10.

Subject headings: pulsars: general — radiation mechanisms: nonthermal — radiation mechanisms: thermal — X-rays: stars

1. INTRODUCTION

Since the launch of the *Compton Gamma Ray Observatory* (*CGRO*), six pulsars have been identified as γ-ray pulsars by EGRET, one (PSR B1509−58) has been identified by OSSE and BATSE (e.g., Nel et al. 1996; Thompson et al. 1996), and possible evidence for identifying PSR B0656+14 as a γ-ray pulsar (Ramanamurthy et al. 1996) has also been obtained. Soft ($\sim$0.1–2.4 keV) X-ray emissions (both unpulsed and pulsed components) from 25 rotation-powered pulsars have so far been detected by *ROSAT*, ten of which have been shown to emit pulsed X-rays (see the review by Becker & Trümper 1997). Furthermore, the *Advanced Satellite for Cosmology and Astrophysics* (*ASCA*) has detected hard (2–10 keV) X-ray emissions from 16 rotation-powered pulsars and obtained the pulsed components of these hard X-rays from some of these pulsars (Saito et al. 1997). *ROSAT* observations indicate an apparently linear relationship between the X-ray luminosity, L_X, of the observed rotation-powered pulsars and their spin-down luminosity, L_{sd}. A similar feature has also been seen in the *ASCA* observations. Combined with *ROSAT* data, X-rays in the range of $\sim$0.1–10 keV from 16 pulsars have been detected so far. It should be pointed out that all known γ-ray pulsars also have X-ray emissions. The observed spectra of X-rays ($\sim$0.1 to $\sim$10 keV) from the several pulsars that are available show that there are at least two kinds of X-ray spectra. One type consists of soft X-rays, which can be fitted by a blackbody spectrum with a single temperature combined with a hard X-ray spectrum with a power-law distribution (for example, the spectra of Geminga and PSR B1055−52). Another type has only a thermal spectrum (for example, PSR B1929+10 and PSR B0950+08). A reasonable explanation is that the soft X-rays have a thermal origin, while the hard X-rays have a nonthermal origin. However, what are the production mechanisms of these thermal and nonthermal X-rays?

There are many possible mechanisms that might explain the soft X-ray emission from pulsars, among them internal frictional dissipation between the stellar crust and the crustal superfluid (Alpar et al. 1984; Shibazaki & Lamb 1989; Cheng et al. 1992), polar-gap heating (e.g., Arons 1981; Harding, Ozernoy, & Usov 1993), outer-gap heating (Cheng 1987; Halpern & Ruderman 1993), accretion from the interstellar medium (Paczyski 1990), accretion of the white dwarf companion onto the neutron star (Edelstein, Foster, & Bowyer 1995), pulsar-wind nebular emission (Arons & Tavani 1993), monopole-catalyzed nucleon decay inside the neutron stars (Freese, Turner, & Schramm 1983), etc. Recently, Zhang & Cheng (1997) proposed a self-consistent outer-gap model for γ-ray emission (a brief review is given in § 3). In this model, they have described the origins of the soft and hard X-rays. Furthermore, Cheng, Gil, & Zhang (1998) developed a model for the nonthermal X-rays based on the model of Zhang & Cheng (1997) in which the nonthermal X-rays come from magnetospheric synchrotron radiation of secondary $e^{\pm}$ pairs produced by high-energy curvature photons in the strong pulsar magnetic field near the neutron star surface. This model can explain the observed relationship between L_X and L_{sd} very well. On the other hand, based on the original outer-gap model (Cheng, Ho, & Ruderman 1986a, 1986b), Wang et al. (1998) also proposed a similar model for X-ray emission

[1] Department of Physics, University of Hong Kong, Pokfulam Road, Hong Kong, China.
[2] Department of Physics, Yunnan University, Kunming, Yunnan, China.

from isolated pulsars. In their model, they divided the isolated pulsars into γ-ray pulsars and non–γ-ray pulsars. For the γ-ray pulsars, 100 MeV curvature γ-rays from electrons or positrons moving toward the star from the outer gap are converted to $e^{\pm}$ pairs on closed field lines all around the star. The nonthermal X-rays are produced by synchrotron radiation of these $e^{\pm}$ pairs, and have a spectral index of ~ 1.5. A cyclotron resonance "blanket" surrounding the star is formed by these $e^{\pm}$ pairs. For the non–γ-ray pulsars, the accelerator (i.e., outer gap) does not exist, and such an optically thick $e^{\pm}$ resonance blanket is not formed. In this case, the blackbody radiation from both the warm stellar surface and the heated polar caps should be directly observable. In this paper we further develop the model of X-ray emissions from the rotation-powered pulsars based on the work of Zhang & Cheng (1997) and Cheng, Gil, & Zhang (1998). The X-ray pulsars are divided into X-ray pulsars with and without outer gaps, and the criteria for separating these two groups is determined by their observed pulsar parameters, i.e., P and B. In § 2, we present the basic observed features of X-ray emissions from the pulsars. In § 3, we describe the model for X-ray pulsars with outer gaps in detail. In particular, the effect of a nondipolar surface magnetic field is emphasized. The model for X-ray pulsars without outer gaps is presented in § 4. A brief discussion of how the viewing angle and the inclination angle affect the observed results is presented in § 5. In § 6, a comparison of model results with observed data is shown. A brief discussion is given in § 7.

2. BASIC OBSERVED CHARACTERISTICS OF X-RAY EMISSIONS FROM PULSARS

Becker & Trümper (1997) presented a homogeneous data set obtained by reanalyzing most of the *ROSAT* observations of pulsars. They listed observed characteristics of 25 pulsars observed by *ROSAT* and two observed by *ASCA*. These pulsars consist of 20 canonical pulsars and seven millisecond pulsars, covering a wide range of ages (10^3 to 7×10^9 yr), surface magnetic fields (10^8 to 10^{13} G), and spin periods (1.6 to 530 ms). In their analysis, the observed energy fluxes, F_X, within the 0.1–2.4 keV band are converted to isotropic luminosities using $L_X = 4\pi d^2 F_X$, where d is the distance to the pulsar. The X-ray luminosities for the total pulsar emission and a pulsed component if detected have been given. The observed data indicate that all pulsars show an X-ray luminosity closely correlated with the rotational energy loss. The best fit shows $L_X(0.1\text{–}2.4 \text{ keV}) \approx 10^{-3} L_{sd}$. From these pulsars, the pulsed X-rays of ten pulsars have been obtained. Moreover, all known γ-ray pulsars have been observed by *ROSAT* to emit X-rays. We list these pulsars in Table 1.

Saito et al. (1997) presented recent observations of pulsars by *ASCA*. Sixteen pulsars (including 14 canonical pulsars and two millisecond pulsars) have been observed to

TABLE 1

BASIC OBSERVED FEATURES OF PULSAR X-RAYS FROM *ROSAT* AND *ASCA*

				ROSAT[a]		*ASCA*[b]	
PULSAR	P (ms)	log B (G)	d (kpc)	log L_X^{obs} (ergs s^{-1})	Pulsed Fraction (%)	log L_X^{obs} (ergs s^{-1})	Pulsed Fraction (%)
B0531+21.....	33.40	12.58	2.00	35.98	74.1	37.02	6.5
B0833−45.....	89.29	12.53	0.50	32.70	10.0	33.28	<3.6
B0633+17.....	237.09	12.21	0.16	31.22	~1	29.79	40
B1706−44.....	102.45	12.49	1.82	33.15	...	32.83	<81
B1509−58.....	150.23	13.19	4.40	34.29	64.6	34.60	33
B1951+32.....	39.53	11.69	2.50	33.44	...	33.79	<14.1
B1046−58.....	123.7	11.54	2.50	...	...	32.96	<66
B1259−63.....	47.76	11.51	2.00	32.95	...	...	...
B1823−13.....	101.45	12.45	4.12	33.39	...	...	...
B1800−21.....	133.61	12.63	3.94	33.06	...	...	...
B1929+10.....	226.51	11.71	0.17	30.00	31.6	30.08	<69
J0437−47	5.75	8.54	0.18	30.98	33.1	30.08	<100
B1821−24.....	3.05	9.35	5.50	33.24	...	33.81	15
B0656+14.....	384.87	12.67	0.76	33.00	10.0	31.23	<100
B0540−69.....	50.37	12.70	49.40	36.21	77.6	36.92	16
J2124−33	4.93	8.36	0.25	30.35	30.9	...	...
B1957+20.....	1.60	8.14	1.53	31.93	...	...	...
B0950+08.....	253.06	11.39	0.12	29.35	...	29.0	<100
B1610−50.....	231.6	13.03	0.12	...	...	34.36	<100
J0538+28	143.15	11.87	1.50	32.74	...	...	...
J1012+53	5.25	8.45	0.52	30.20	...	...	...
B1055−52.....	197.10	12.03	0.50	32.83	12.6	30.43	<100
B0355+54.....	156.38	11.92	2.07	31.96	...	...	...
B2334+61.....	495.24	12.99	2.46	31.86	...	...	...
J0218+42	2.32	8.63	5.70	32.75	...	...	...
B0823+26.....	530.66	11.99	0.38	29.83	...	...	...
J0751+18	3.47	8.23	2.02	31.60	...	...	...
B1853+01.....	267.4	12.88	2.02	...	...	33.15	<10

[a] Energy range is from 0.1–2.4 keV. Data are from Becker & Trümper (1997).
[b] Energy range is from 2–10 keV. Data are from Saito et al. (1997).

emit hard (0.7–10 keV) X-rays. In addition to the total fluxes of X-rays, the pulsed fluxes, or upper limits, of these pulsars are also given. They found an empirical relation between the pulsed luminosity, L_X^{pulse}, and the rotation energy loss, L_{sd}, in the X-ray band for all X-ray pulsars, i.e., $L_X^{pulse} \propto L_{sd}^{3/2}$. Combined with the *ROSAT* observations, 16 pulsars have been detected to emit X-rays from 0.1–10 keV. It should been noted that all known γ-ray pulsars have also been detected to emit X-rays from 0.1 to 10 keV. The observed characteristics of these 16 pulsars are shown in Table 1.

Although 27 pulsars have been detected to emit X-rays, the detailed spectral structure of few pulsars can be found in the literature. Halpern & Ruderman (1993) presented the X-ray spectrum of Geminga from an analysis of the *ROSAT* observations. Recently, Halpern & Wang (1997) studied the X-ray emission from Geminga at energies of 0.1–10 keV using data from the *ASCA*, *ROSAT*, and *Extreme-Ultraviolet Explorer* (*EUVE*) satellites. The X-ray spectrum from Geminga appears to have two components. One is a soft thermal X-ray spectrum with a temperature of $T_s = (5.6 \pm 0.6) \times 10^5$ K. The other is a nonthermal hard X-ray spectrum with a spectral index of 2.0 ± 0.5. The hard X-ray light curve has a strong main peak and a weak secondary peak; its total pulsed fraction is $\sim 55\%$. The X-ray spectrum of PSR B1055–52 has been detected (Ögelman & Finley 1993; Greiveldinger et al. 1996); it can also be fitted with a blackbody distribution with a temperature of $T_s = 7.9^{+0.6}_{-1.0} \times 10^5$ K and a nonthermal power law distribution with a spectral index of 1.5 ± 0.3 (Wang et al. 1998). *ROSAT* and *ASCA* observations of PSR B0656+14 have also been presented (e.g., Possenti, Mereghetti, & Colpi 1996; Greiveldinger et al. 1996). This pulsar features, at minimum, two components: a thermal component with a temperature of $\sim 8 \times 10^5$ K, and a nonthermal component with a spectral index of 1.5 ± 1.1 (Greiveldinger et al. 1996). Furthermore, Wang & Halpern (1997) presented *ASCA* X-ray spectra of PSR B1929+10 and PSR B0950+08, and pointed out that they can be fitted to simple blackbodies with temperatures of $(5.14 \pm 0.53) \times 10^6$ K for PSR B1929+10 and $(5.7 \pm 0.63) \times 10^6$ K for PSR B0950+08, respectively. However, Wang et al. (1998) have pointed out that the X-ray data of PSR B0950+08 given by Wang & Halpern (1997) are incorrect, because the measurements are heavily contaminated by an active galactic nucleus (AGN) that lies within the X-ray error box. We summarize the observed spectral characteristics of these pulsars in Table 2. The most interesting result is that the γ-ray pulsars with effective blackbody emission areas are near 100 times larger than the polar-cap area deduced by the dipolar field, but non–γ-ray pulsars with the effective area have ~ 100 times less than the polar-cap area.

3. X-RAY EMISSION ORIGINATING FROM THE BACKFLOW CURRENT OF THE OUTER GAP

In this section, we describe those X-ray components that result from the return current of the outer gap. We will use the self-consistent model of the outer gap for γ-ray emission from the pulsar proposed by Zhang & Cheng (1997), the basic features of which are as follows.

1. The $e^{\pm}$ pairs needed to control the size of the outer gap are produced by photon-photon pair production resulting from collisions between the curvature photons from the gap and thermal X-rays from the neutron star surface. These thermal X-rays are produced by the collision of the backflowing current with the neutron star surface. Although the X-ray photon density is very low, every pair produced by X-ray and curvature photons' collision can emit 10^5 photons in the gap. Such a huge multiplicity can produce a sufficient number of $e^{\pm}$ pairs to sustain the gap as long as the center of mass energy of the X-ray and curvature photon is higher than the threshold for electron-positron pair production, i.e., $E_X E_\gamma \geq (m_e c^2)^2$. From the condition for photon-photon pair production, the size of the outer gap, which is the ratio between the potential drop of the outer gap and the total potential of the open field lines (Zhang & Cheng 1997), limited by the soft thermal X-rays from the neutron star surface, can be determined as

$$f = 5.5 P^{26/21} B_{12}^{-4/7} . \quad (1)$$

It should be emphasized that $f \leq 1$ if the outer gap exists. Any fluctuation of the gap can be stabilized by the process described above. In fact, an increase in the gap size will increase the X-ray flux, and the overproduced pairs in turn will reduce the gap size. Similarly, a decrease of the gap size will result in insufficient pairs, which in turn will increase size of the gap.

2. The primary $e^{\pm}$ pairs in the steady state have a power-law distribution with a spectral index of 16/3, because the Lorentz factor of the accelerated particles in the outer gap is $\gamma(x) \propto x^{-3/4}$, where $x = s/R_L$, s is the local radius of curvature, and R_L is the radius of the light cylinder.

3. The γ-rays are produced by the synchro-curvature radiation (Cheng & Zhang 1996) in the outer gap, which depends sensitively on the local curvature. Therefore, the radiation spectrum produced by the accelerated particles with a power-law distribution in the outer gap depends on two parameters, x_{min} and x_{max} (Zhang & Cheng 1997). The quantity x_{min} depends on the distance from the center of the pulsar to the inner boundary of the outer gap, r_{in}. Generally, r_{in} is determined by both the structure of the magnetic field in the pulsar magnetosphere and the inclination angle χ between the stellar moment and the spin axis. When the inclination angle χ is large, then $r_{in} \approx (4/9) R_L / \tan^2 \chi$

TABLE 2

BASIC OBSERVED SPECTRAL FEATURES OF X-RAY PULSARS

Pulsar	T_s (10^5 K)	T_h (10^6 K)	N_H (10^{20} cm^{-2})	log L_{sX}^{obs} (ergs s^{-1})	log L_{hX}^{obs} (ergs s^{-1})	Spectral Index	Reference
B0633+17.....	5.77	...	1.14	31.17	29.91	0.47 ± 0.25	1
B1055−52.....	7.9	...	2.6	32.36	30.18	0.5 ± 0.3	2
B0656+14.....	7.8	...	1.7	32.63	31.23	0.50 ± 0.37	3
B1929+10.....	...	5.14	...	...	30.11	...	4

REFERENCES.—(1) Halpern & Wang 1997; (2) Wang et al. 1998; (3) Greiveldinger et al. 1996; (4) Wang & Halpern 1997.

(Halpern & Ruderman 1993), and

$$x_{\min} \sim \tfrac{2}{3}(\tan \chi^{-1}) . \quad (2)$$

The quantity $x_{\max}$ depends on χ and f. For a very thick outer gap and a nearly aligned rotator, $x_{\max} \sim 2$. Furthermore, when the particle energy density is comparable to that of the local magnetic energy density, the local radius of curvature can become larger.

From these basic features, we can see that a pulsar is a γ-ray pulsar if f (eq. [1]) is less than unity. Otherwise, the pulsar will be a non–γ-ray pulsar and its X-ray emission, if any, should be thermal (see § 4). In this section we will first consider the X-ray emission originating from a pulsar with outer gaps. We will show that the X-ray luminosity produced by polar-cap heating of the polar gap is always less than that produced by return current from the outer gaps; the reason for this will be presented in § 4. Figure 1 shows a schematic description of our model for X-ray emission. The details of our model are described below. (As a good approximation for the particles outside the outer gap, we will use curvature radiation instead of synchro-curvature radiation.)

3.1. *Backflowing High-Energy Electrons/Positrons from the Outer Gap*

Half of the primary electrons/positrons in the outer gap will move toward the star and lose their energy via curvature radiation. The Lorentz factor of the $e^{\pm}$ at the inner boundary of the outer gap can be approximated as (Zhang & Cheng 1997)

$$\gamma(x_{\min}) \approx 2.8 \times 10^7 f^{1/2} B_{12}^{1/4} P^{-1/4} x_{\min}^{-3/4} . \quad (3)$$

These electrons/positrons leaving the outer gap emit curvature photons with a characteristic energy of

$$E_\gamma = \frac{3}{2} \hbar \frac{c}{s} \gamma(x_{\min})^3 \approx 136.3 f^{3/2} P^{-7/4} B_{12}^{3/4} x_{\min}^{-13/4} \text{ MeV} . \quad (4)$$

The energy loss by curvature radiation is $mc^2(d\gamma/dt) = -(2/3)(e^2c/s^2)\gamma^4$. If the magnetic field is dipolar, $s^2 \approx rR_L$ and $r \approx ct$, and the Lorentz factor of return particles at the distance r is given by $\gamma(r) = \gamma(r_{\rm in})\{1 + [2e^2\gamma(r_{\rm in})^3/R_L mc^2] \ln (r_{\rm in}/r)\}^{-1/3}$, where $\gamma(r_{\rm in}) = \gamma(x_{\min})$. Near the neutron star surface, $(r \sim R)$, $\gamma(r)^3 \ll \gamma(r_{\rm in})^3$; then we have

$$\gamma(r) \approx 1.5 \times 10^7 P^{1/3} \left[\ln \left(x_{\min}^2 \frac{R_L}{r} \right) \right]^{-1/3} , \quad (5)$$

which depends on the period and inclination angle of the pulsar. This means that an energy equal to

$$E_e(R) = mc^2\gamma(R) \approx 12.3 P^{1/3} \left[\ln \left(x_{\min}^2 \frac{R_L}{R} \right) \right]^{-1/3} \text{ ergs s}^{-1} \quad (6)$$

will deposit on the stellar surface, although most of the energy of the primary particles will be lost on the way to the star via curvature radiation.

The return particle flux can be approximated as

$$\dot{N}_e = f\dot{N}_{\rm GJ} \approx 2.7 \times 10^{30} f B_{12} P^{-2} R_6^3 , \quad (7)$$

where $\dot{N}_{\rm GJ}$ is the Goldreich-Julian particle flux (Goldreich & Julian 1969), and R_6 is the radius of the neutron star in units of 10^6 cm. These high-energy $e^{\pm}$ pairs will radiate most of their energy when they move toward the stellar surface. Some of the high-energy photons radiated by the return particles will be converted into secondary $e^{\pm}$ pairs near the neutron star if the pair production condition in the strong magnetic field is satisfied (Erber 1966; Ruderman & Sutherland 1975, hereafter RS), i.e., if

$$\frac{E_\gamma}{2mc^2} \frac{B(r_s)}{B_g} \approx \frac{1}{15} , \quad (8)$$

where $B(r_s)$ is the local magnetic field at position r_s, and $B_g = m^2c^3/e\hbar \approx 4.4 \times 10^{13}$ G. From this condition, and assuming that the local field is a dipole field, the distance, r_s, from the star of the first generation of secondary $e^{\pm}$ pairs can be estimated by

$$\frac{r_s}{R} = \left(\frac{15 E_\gamma B_s}{2mc^2 B_g} \right)^{1/3} \approx 0.6 B_{12}^{1/3} \left(\frac{E_\gamma}{mc^2} \right)^{1/3} \quad (9)$$

where E_γ is given by equation (4) and B_s is the surface magnetic field. At this position, each electron and positron carries about half the parent γ-ray energy, and quickly loses its momentum perpendicular to the local magnetic field of synchrotron radiation. The characteristic energy produced by synchrotron radiation at r_s is given by $E_{\rm syn} = E_\gamma/20$ (Cheng, Gil, & Zhang 1998). Since these synchrotron photons are emitted toward the star, they will encounter a stronger magnetic field and convert further into $e^{\pm}$ pairs; these pairs radiate their energies through synchrotron radi-

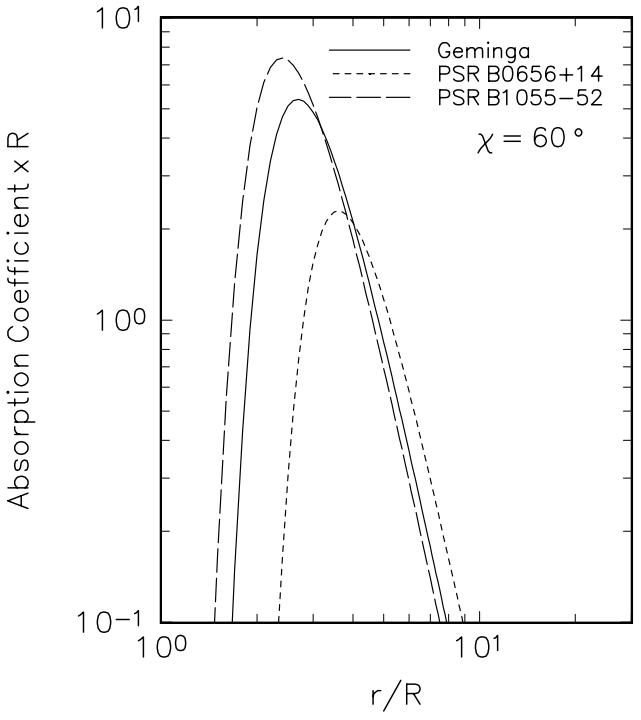

FIG. 1.—Schematic illustration of X-rays produced by the backflow current from the outer gap. The return current from the outer gap will heat the stellar surface and emit hard thermal X-rays. Part of the hard thermal X-rays will be reflected back to the entire stellar surface in the closed magnetic field lines and then reradiate as soft thermal X-rays. The hard thermal X-rays in the open magnetic field lines will escape and therefore be modulated. On the other hand, nonthermal X-rays will be produced by synchrotron radiation of secondary $e^{\pm}$ pairs that are created by the curvature photons emitted by primary particles from the outer gap.

ation again. Therefore, a cascade can develop. It can be easily shown that the relations between positions and Lorentz factors of ith and $(i+1)$th generations of $e^{\pm}$ pairs are $(r_{i+1}/r_i) = (1/20)^{1/3}$ and $\gamma_{i+1}/\gamma_i = 1/20$, respectively (Cheng et al. 1998). Therefore, the position at which the pair-production process stops can be written as

$$\frac{r_f}{R} = \left(\frac{1}{20}\right)^{n_f/3} \frac{r_s}{R}, \tag{10}$$

where n_f is the generation number. The photon energy at r_f can be written as

$$E_f = \left(\frac{1}{20}\right)^{n_f} E_{\rm syn}. \tag{11}$$

The production rate of the secondary $e^{\pm}$ pairs produced at the position r_s in this way is given by (Zhang & Cheng 1997)

$$\dot{N}_{e^{\pm}}^{(1)} \approx 3.3 \times 10^{30} f^{-1/2} B_{12}^{5/4} P^{-17/4} x_{\rm min}^{-19/4} \left(\frac{r_s}{R}\right)^2 \ {\rm s}^{-1}. \tag{12}$$

According to Zhang & Cheng (1997), there is another source of secondary $e^{\pm}$ pairs originating from the primary γ-rays from the outer gap. A portion of these photons will be converted into $e^{\pm}$ pairs in both open and closed magnetic field line regions near the neutron star through the mechanism of magnetic pair creation. At the position r_s, the primary γ-rays are converted into $e^{\pm}$ pairs; the number rate of $e^{\pm}$ at the distance r_s can be approximated as

$$\dot{N}'_{e^{\pm}} \approx \frac{P_{\rm gap}}{E_\gamma} \left(\frac{r_s}{R_L/2}\right)^2 \frac{\pi}{\Delta\Omega}, \tag{13}$$

where $\Delta\Omega$ is the solid angle of the primary γ-ray beam (we assume that $\Delta\Omega = 1$ sr), E_γ is given by equation (4), and $P_{\rm gap}$ is the power provided by the outer gap, which is $\sim 3.6 \times 10^{31} f^3 P^{-4} B_{12}^2$ ergs s^{-1}. These relativistic $e^{\pm}$ pairs will emit high-energy photons in the direction of the star, where the magnetic field is increasing rapidly, and their energies are sufficiently high to make further generation of $e^{\pm}$ pairs possible, which then form the cascade described above until their Lorentz factors approach unity. The resulting flux of the pairs can be written as (Zhang & Cheng 1997)

$$\dot{N}_{e^{\pm}}^{(2)} \approx \frac{E_\gamma}{\rm MeV} \dot{N}'_{e^{\pm}} \approx 2.5 \times 10^{31} f^3 P^{-6} B_{12}^2 \left(\frac{r_s}{R}\right)^2 \ {\rm s}^{-1}. \tag{14}$$

Therefore, the number density of these $e^{\pm}$ pairs at the distance r from the star can be estimated as

$$n_{e^{\pm}} \approx \frac{1}{4\pi r^2 c} [\dot{N}_{e^{\pm}}^{(1)} + \dot{N}_{e^{\pm}}^{(2)}]. \tag{15}$$

3.2. *The Thermal X-Ray Production*

The luminosity of thermal X-rays from the stellar surface resulting from the bombardment of the return current is given by

$$L_{\rm X} = E_e(R)\dot{N}_e \approx 3.3 \times 10^{31} f B_{12} P^{-5/3} \times \left[\ln\left(x_{\rm min}^2 \frac{R_L}{R}\right)\right]^{-1/3} {\rm ergs\ s}^{-1}, \tag{16}$$

where $E_e(R)$ is given by equation (6). The corresponding characteristic temperature is given by

$$T_h = \left(\frac{L_{\rm X}}{A\sigma_{\rm SB}}\right)^{1/4}, \tag{17}$$

where A is the area of the stellar surface bombarded by the return current ($A \sim \pi f \Omega R^3/c$ for a dipole magnetic field), and $\sigma_{\rm SB}$ is Stefan's constant. These X-rays have a blackbody distribution. However, whether or not these X-rays can escape from the stellar surface depends on the cyclotron-resonant X-ray reflecting mirror. We describe this process as follow.

The differential number density of hard X-rays with a blackbody distribution is given by

$$n(\omega)\, d\omega = \frac{\omega^2\, d\omega}{\pi^2 c^3 (e^{\hbar\omega/kT_h} - 1)}, \tag{18}$$

where ω is the angular frequency of the X-ray photons and T_h is given by equation (17). These X-ray photons will be effectively scattered as a result of resonant cyclotron scattering by the $e^{\pm}$ plasma screen on the strong magnetic field lines. The cross section is given by (Halpern & Ruderman 1993)

$$\sigma = \sigma_{\rm T}(\hat{\mathscr{E}} \cdot \hat{B})^2 + \frac{2\pi^2 e^2}{mc} |\hat{\mathscr{E}} \times \hat{B}|^2 \delta(\omega_B - \omega), \tag{19}$$

where $\hat{\mathscr{E}}$ is the photon polarization, $\sigma_{\rm T}$ is the Thomson cross section, and $\omega_B = eB(r)/mc$. The absorption coefficient $\tau(r)$ can be expressed as

$$\tau(r) = \int n_{e^{\pm}} \sigma \left[\frac{n(\omega)\, d\omega}{\int_0^\infty n(\omega)\, d\omega}\right]. \tag{20}$$

In general, the cross section depends on the angle between polarizations of the electric and magnetic fields. However, in the closed field line region of the magnetosphere, the condition of $\hat{\mathscr{E}} \cdot \hat{B} \sim 0$ is satisfied. In this case, the hard X-rays are effectively scattered, because the optical depth is much larger than unity. In fact, the expression given in equation (20) for $\hat{\mathscr{E}} \cdot \hat{B} \sim 0$ can be approximated as

$$\tau(r) = 0.3 \left(\frac{B_{12}^2}{T_6^3}\right) \{[\dot{N}_{e^{\pm}}^{(1)}]_{37} + [\dot{N}_{e^{\pm}}^{(2)}]_{37}\} \times \frac{(r/R)^{-8}}{e^{[(\hbar\omega_0)/(kT_h)](r/R)^{-3}} - 1} \ {\rm cm}^{-1}, \tag{21}$$

where $\omega_0 = eB_s/mc \approx 1.8 \times 10^{19} B_{12}$ s^{-1}, $T_6 = T_h/10^6$ K, and $[\dot{N}_{e^{\pm}}^{(1)}]_{37}$ and $[\dot{N}_{e^{\pm}}^{(2)}]_{37}$ are in units of 10^{37} s^{-1}. From equation (21), the distance r_a at which the absorption coefficient approaches a maximum, $\tau_{\rm max}$, can be easily obtained, i.e., $r_a/R \sim 3.8(B_{12}/T_6)^{1/3}$ if $(\hbar\omega_0/kT_h)(r_a/R)^{-3} \gg 1$. On the other hand, in the open field line region near the stellar surface, the condition of $\hat{\mathscr{E}} \times \hat{B} \sim 0$ may be satisfied because there may be an acceleration region at the polar cap. In this case, the hard X-rays may escape from the polar cap as a result of the negligible optical depth (Halpern & Ruderman 1993). Generally, a portion of the hard X-rays produced at the polar cap will escape along the open magnetic field lines; their temperature is determined by equation (17), and their luminosity is given by

$$L_{\rm X}^h = \xi L_{\rm X}, \tag{22}$$

where ξ represents the ratio of the hard X-ray luminosity to the X-ray luminosity given by equation (16). These thermal hard X-rays will be modulated, because they escape mainly along the open magnetic field lines with half-open angle θ_h. In an aligned rotator,

$$\theta_h \sim \left(\frac{r_s}{R_L}\right)^{1/2} \tag{23}$$

and $\xi = \theta_h^2$. For $P = 0.1$ s, $\xi \sim 0.1$. For a nonaligned rotator, although it is not clear whether the secondary cascade $e^{\pm}$ pairs can cover the entire closed field line regions, θ_h could be estimated as

$$\theta_h \sim \frac{r_f}{r_s} = \left(\frac{1}{20}\right)^{n_f/3} . \tag{24}$$

Therefore, we have

$$\xi \sim \max\left[\frac{r_s}{R_L}, \left(\frac{1}{20}\right)^{2n_f/3}\right]. \tag{25}$$

In most cases, only a small percentage of hard X-rays can escape through a narrow window with opening angle $\leq 10^\circ$. Therefore, most of the hard X-rays produced at the polar cap will be reflected back to the surface of the neutron star in the closed magnetic field lines; their energies will be transferred to the entire surface of the neutron star, then be reradiated away in the form of soft X-rays. In this way, the soft X-ray luminosity can be expressed as

$$L_{\rm X}^s = (1 - \xi)L_{\rm X} . \tag{26}$$

The temperature of these soft X-rays is given by

$$T_s = \left[\frac{L_{\rm X}^s}{4\pi R^2 \sigma_{\rm SB}}\right]^{1/4} . \tag{27}$$

Finally, the soft X-rays will escape. It should be pointed out that the fractional size of the outer gap, f, will be changed by a factor of $(1 - \xi)^{1/7}$ when equation (27) is used.

3.3. *The Effect of a Strong Local Surface Magnetic Field*

It is generally believed that a global dipole magnetic field exists in the pulsar magnetosphere (e.g., Gil & Cheng 1998). However, the dipole magnetic field may not describe the surface field, although it gives a good description of the magnetic field far from the star. One possibility is that a multipole magnetic field exists near the stellar surface. In fact, RS assumed that there should be a strong multipolar surface magnetic field, with a radius of curvature $\sim 10^6$ cm, in order to explain the copious γ-B pair-production process. Theoretically, it has been argued that the neutron star magnetic field is produced by currents flowing in a thin crustal layer of thickness $\Delta r \ll R$, where $R = 10^6$ cm is the neutron star radius (e.g., Blandford, Applegate, & Hernquist 1983; Romani 1990). Thus, the actual surface magnetic field should be dominated by multipoles of the order of $l \sim R/\Delta r \gg 1$. Arons (1993) suggested that the surface magnetic field should be a superposition of clumps covering the whole surface of a neutron star. The surface magnetic field can be approximated by $B_s \sim B_d(R/\Delta r)^n$, where B_d is the surface dipole component, which can be inferred from the pulsar spin down rate, and $n = 1$ and 2 represent coherent and incoherent superpositions of dipole moments of clumps, respectively. In this case, the surface magnetic field is always greater than the surface dipole component.

According to Ruderman (1991a, 1991b, 1991c), however, the surface magnetic field evolution of a pulsar follows the changes in the magnetic field in the core that are caused by the strong interaction between the spinning superfluid neutrons and magnetized superconducting protons in the core. When a pulsar spins down or spins up, the crustal platelets can be pulled by strong shearing stresses. These stresses will strain the crust beyond its yield strength and then cause the crust to move, carrying with it an embedded surface magnetic field. Consequently, "sunspot-like" clumps of the magnetic field at the stellar surface can result from the motion of crustal platelets. The surface magnetic field depends on whether the pulsar spins down or spins up.

If a strong local surface magnetic field (B_s) exists, there are two important effects. The first is that the potential drop of the polar gap should be reduced (see § 4). The other effect is that the surface magnetic field will change the polar-cap area compared to the area of the dipole magnetic field B_d. We consider two possible cases. In the first case, there are only polar gaps in the pulsar magnetosphere (e.g., old pulsars). From magnetic flux conservation, the polar-cap area, determined by open magnetic field lines penetrating the light cylinder, is given by

$$A_p = \frac{B_d}{B_s} A_d , \tag{28}$$

where A_d is the polar-cap area for the dipolar magnetic field B_d, and A_p is the actual polar-cap area, which will be smaller than A_d for a strong surface magnetic field B_s. In the second case, there are also outer gaps in the pulsar magnetosphere, in addition to the polar gaps. If there is a strong multipole surface magnetic field located in a region near the polar cap, with typical dimensions and a typical radius of curvature l that is much less than the dipolar radius s of curvature of a dipolar field near stellar surface, at some point a distance δr above the stellar surface, the surface magnetic field is equal to the dipole magnetic field, i.e.,

$$B_s^0\left(\frac{l + \delta r}{l}\right)^{-(m+1)} = B_d^0\left(\frac{R + \delta r}{R}\right)^{-3} , \tag{29}$$

where B_s^0 and B_d^0 are the surface and dipole fields at the stellar surface, and $m = 2$ means that the surface magnetic field is a localized dipole field, e.g., a sunspot structure. From this equation, we have

$$\frac{\delta r}{l} \sim \left(\frac{B_s^0}{B_d^0}\right)^{1/(m+1)} - 1 \tag{30}$$

if $B_s^0/B_d^0 \gg 1$. Most of the energy of the return particles, given in equation (6), will not be deposited on the polar area (eq. [28]); instead, many curvature photons will be produced around δr above the surface if l is much less than the radius of curvature of the dipole magnetic field B_d, and then many $e^{\pm}$ pairs will be created by the magnetic pair production process in the strong surface magnetic field. Therefore, a cascade will develop. The area over which the $e^{\pm}$ pairs collide with the stellar surface is estimated as

$$A_{\rm eff} \sim (\delta r)^2 , \tag{31}$$

which depends on the ratio of B_s^0 to B_d^0. This means that $A_{\rm eff} \gg A_d \gg A_p$ for pulsars with outer gaps and a strong surface magnetic field. For this case, the temperature of

thermal X-ray emission is always given by

$$T_h^m = \left(\frac{A_d}{A_{\rm eff}}\right)^{1/4} T_h \,, \tag{32}$$

where T_h is the temperature of the thermal X-rays when the surface magnetic field effect is ignored. T_s in equation (27), however, remains unchanged.

3.4. *The Nonthermal X-Ray Production*

As described in § 3.1, the primary electrons/positrons leaving the outer gap emit curvature photons, which will be converted into secondary $e^{\pm}$ pairs by the neutron star magnetic field at a position r_s, given by equation (9). Subsequently, these $e^{\pm}$ pairs lose their energies rapidly via synchrotron radiation, with typical photon energy $E_{\rm syn}$. The synchrotron photons will be further converted into $e^{\pm}$ pairs if their energies are large enough. Such a process can repeat at least one more time before the synchrotron photon energy reduces to E_f (eq. [11]) and then produces nonthermal X-rays. We take Geminga as an example; for the parameters of Geminga, i.e., $P = 0.237$ s, $B_{12} = 1.6$, and $x_{\rm min} = 0.3$, equation (4) gives the energy of the curvature photons as $E_\gamma = 25.6$ GeV, the position of the first generation of $e^{\pm}$ pairs as $r_s/R = 24.0$, and the energy of the first generation of synchrotron radiation as $E_{\rm syn} \sim 1.28$ GeV. Since these synchrotron photons are emitted toward the star, they will encounter a stronger magnetic field and convert into $e^{\pm}$ pairs, which again radiate their energy via synchrotron radiation. Because each new generation of $e^{\pm}$ pairs will have their energy reduced by a factor of ~ 0.05 and come closer to the star by a factor of ~ 0.37, it takes about two generations to reduce their energy to 1.28 GeV $\times$ $(0.05)^2$ MeV $\sim$ 3.2 MeV, and the pair production processes stops at $r_f/R \sim (r_s/R)(1/20)^{2/3} \sim 3.3$. The synchrotron spectral index starts with $-\beta_i = -1.5$ and evolves to become $-\beta_f = -[1 + (1 + \beta_i/2)/2] \sim -1.9$.

3.5. *The X-Ray Spectrum and Luminosity*

In our model, the outer gap can produce two thermal components and one nonthermal component on or near the neutron star surface. Of the two thermal components, one is soft thermal X-rays, with a temperature given by equation (27) and a spectrum that can be written as

$$\frac{d\dot{N}_{\rm sX}^{\rm thermal}}{dE_{\rm X}} = A_s \frac{(E_{\rm X}/mc^2)^2}{e^{E{\rm X}/kT_s} - 1} \,, \tag{33}$$

where A_s depends on the luminosity of the thermal X-rays (eq. [26]) and is given by

$$A_s = \frac{15}{\pi^4}\frac{(mc^2)^2}{(kT_s)^4} L_{\rm X}^s \,. \tag{34}$$

The other component is hard thermal X-rays with a temperature given by equation (17) or equation (32). Because part of the hard thermal X-rays can escape along the open magnetic field lines, the hard X-rays will be modulated. In fact, if $\alpha(t)$ is the angle between the magnetic axis and the line of sight, it is given by

$$\cos\,\alpha(t) = \cos\,\chi\,\cos\,\zeta + \sin\,\chi\,\sin\,\zeta\,\cos\,(\Omega t) \,, \tag{35}$$

where χ is the inclination angle, ζ is the angle between the rotation axis and the line of sight, $\Omega = 2\pi/P$, and t is the time. Therefore, as the star rotates, $\alpha(t)$ changes and the emission is modulated. In principle, the hard thermal X-rays can be observed if $|\zeta - \chi| \le \theta_h$. The spectrum of the hard thermal X-rays in this case can be expressed as

$$\frac{d\dot{N}_{\rm hX}^{\rm thermal}}{dE_{\rm X}} = A_h \frac{(E_{\rm X}/mc^2)^2}{e^{E{\rm X}/kT_h} - 1} \,, \tag{36}$$

where

$$A_h = \frac{15}{\pi^4}\frac{(mc^2)^2}{(kT_s)^4} L_{\rm X}^h \langle \cos\,\alpha(t)\rangle \,. \tag{37}$$

For the nonthermal X-rays, assuming that the distribution of the $e^{\pm}$ pairs produced by curvature radiation can be approximated by a δ function, the steady state spectrum is proportional to E_e^{-2}. We argue that an electromagnetic cascade will continue until the energy of synchrotron photons is $\sim$MeV, so that the spectral index of the nonthermal X-rays should be ≤ 2. Furthermore, the total number of secondary $e^{\pm}$ pairs created in the electromagnetic cascade is given by equation (12). Therefore, the luminosity of nonthermal X-rays produced by the cascade is given by

$$L_{\rm X}^n \approx 1.4 \times 10^{24} f^{-1/2} B_{12}^{5/4} P^{-17/4} \left(\frac{r_s}{R}\right)^2 x_{\rm min}^{-19/4} \text{ ergs s}^{-1} \,. \tag{38}$$

In the case of millisecond pulsars, for which the light cylinder is much closer to the star than that in canonical pulsars, we must use $r_s \approx R$ (the much stronger multipole surface magnetic field will allow copious pair production there) and

$$L_{\rm X,ms}^n \sim 1.4 \times 10^{24} f^{-1/2} B_{12}^{5/4} P^{-17/4} x_{\rm min}^{-19/4} \text{ ergs s}^{-1} \,. \tag{39}$$

The spectral index of millisecond pulsars should be 1.5. The spectrum of nonthermal X-rays can be expressed as

$$\frac{d\dot{N}_{\rm hX}}{dE_{\rm X}} = A_n \left(\frac{E_{\rm X}}{\rm MeV}\right)^{-\beta_f} \quad \text{for } E_{\rm X,min} \le E_{\rm X} \lesssim \text{MeV} \,, \tag{40}$$

where β_f is the spectral index at position r_f (where the electromagnetic cascade stops), and $E_{\rm X,min}$ is the minimum energy of nonthermal X-rays, which can be expressed as

$$E_{\rm X,min} = \hbar[eB(r_f)/mc] \approx 1.1 \times 10^4 B_{12}(r_f/R)^{-3} \text{ eV} \,. \tag{41}$$

The normalized coefficient, A_n, is given by

$$A_n \approx L_{\rm X}^n \begin{cases} (2 - \beta_f)/\{[1 - (E_{\rm X,min}/E_0)^{2-\beta_f}]E_0^2\} & \text{for } \beta_f < 2 \,, \\ [E_0^2 \ln\,(E_0/E_{\rm X,min})]^{-1} & \text{for } \beta_f = 2 \,, \end{cases} \tag{42}$$

where $E_0 = 1$ MeV.

The total (thermal and nonthermal) luminosity and spectrum of the X-rays originating from the outer gap depends on the inclination angle and viewing angle of the pulsar. Generally, if the viewing angle is close to the inclination angle (i.e., $|\zeta - \chi| \le \theta_h$), we have

$$L_{\rm X}^t = L_{\rm X}^s + L_{\rm X}^h + L_{\rm X}^n \tag{43}$$

and

$$\frac{d\dot{N}_{\rm X}}{dE_{\rm X}} = \frac{d\dot{N}_{\rm sX}^{\rm thermal}}{dE_{\rm X}} + \frac{d\dot{N}_{\rm hX}^{\rm thermal}}{dE_{\rm X}} + \frac{d\dot{N}_{\rm hX}}{dE_{\rm X}} \,, \tag{44}$$

TABLE 3

EXPECTED QUANTITIES OF X-RAY PULSARS[a]

Pulsar	T_s (10^5 K)	T_h (10^6 K)	T_h^m (10^6 K)	E_γ (GeV)	(r_s/R)	$r_a\ \alpha(r_a)$
B0531+21.....	8.4	8.3	7.3	12.8	25.3	4.0×10^5
B0833−45.....	7.3	6.7	4.6	14.4	25.3	3.4×10^3
B0633+17.....	6.0	4.6	2.5	17.3	21.1	14.5
B1706−44.....	7.1	6.3	4.3	14.8	24.8	1.5×10^3
B1509−58.....	8.0	8.8	5.4	12.9	40.6	3.5×10^3
B1951+32.....	6.6	4.8	4.1	16.2	13.8	6.5×10^3
B1046−58.....	7.0	6.3	4.0	14.9	25.8	7.7×10^2
B1259−63.....	6.1	4.2	3.4	17.3	12.3	1.4×10^3
B1823−13.....	7.0	6.2	4.2	14.9	24.1	1.4×10^3
B1800−21.....	7.1	6.6	4.1	14.7	27.5	7.5×10^2
J0437−47	4.0	1.2	1.6	28.7	1.5	7.6×10^2
B1821−24.....	5.5	2.1	3.5	22.0	2.5	1.5×10^5
B0656+14.....	6.3	5.5	2.7	16.3	29.4	8.3
B0540−69.....	8.2	8.2	6.6	13.0	27.9	9.1×10^4
J2124−33	3.9	1.1	1.5	29.5	1.3	8.4×10^2
B1957+20.....	5.0	1.4	2.6	27.6	1.1	3.3×10^4
B1610−50.....	7.3	7.5	4.1	14.1	36.9	2.6×10^2
J0538+28	5.8	4.2	2.6	17.8	16.4	39.5
J1012+53	4.0	1.1	1.6	29.1	1.4	8.4×10^2
B1055−52.....	5.8	4.3	2.5	17.7	18.5	17.6
B0355+54.....	5.8	4.2	2.6	17.8	17.0	32.1
B2334+61.....	6.6	6.3	2.7	15.4	36.9	8.0
J0218+42	4.9	1.5	1.6	25.5	1.5	3.7×10^4
J0751+18	4.0	1.1	1.7	29.4	1.2	2.0×10^3
B1853+01.....	6.9	6.7	3.5	14.9	33.5	78.9

[a] We assume that all X-ray pulsars have an inclination angle of 60°, and that the typical radius of curvature for the surface magnetic field is about 10^5 cm.

respectively. Otherwise, the luminosity (spectrum) of the X-rays only consists of the soft thermal X-rays and nonthermal X-rays. If we estimate the luminosity of X-rays with energy ranges from E_1 to E_2, we have

$$L_X^{s,h}(E_1 < E_X < E_2) = L_X^{s,h}\left(\frac{15}{\pi^4}\int_{z1}^{z2}\frac{z^3\,dz}{e^z-1}\right) \qquad (45)$$

for the thermal X-rays, where $z1 = E_1/kT_s$ and $z2 = E_2/kT_s$ for soft thermal X-rays, and $z1 = E_1/kT_h$ and $z2 = E_2/kT_h$ for hard thermal X-rays. In addition,

$$L_X^n(E_1 < E_X < E_2) = \begin{cases} \left(\dfrac{E_2}{E_0}\right)^{2-\beta_f}\dfrac{1-E_1/E_2^{2-\beta_f}}{1-(E_{X,\min}/E_0)^{2-\beta_f}} & \text{for } \beta_f < 2\,, \\ \dfrac{\ln\,(E_2/E_1)}{\ln\,(E_0/E_{X,\min})} & \text{for } \beta_f = 2 \end{cases} \qquad (46)$$

for nonthermal X-rays. In order to estimate the flux on the Earth, the interstellar absorption must be taken into account, although it can be ignored above ~ 0.5 keV. The differential energy flux on the Earth can be written as

$$F_X(E_X) = \frac{1}{4\pi d^2}\frac{d\dot{N}_X}{dE_X}\exp\,[-\sigma(E_X)N_H]\,, \qquad (47)$$

where d is the distance to the pulsar, $\sigma(E_X)$ is the photoelectric cross section of the interstellar medium (Morrison & McCammon 1983), and N_H is the interstellar column density. The integrated energy flux over the energy region from E_1 to E_2 on the Earth can be expressed as

$$F_X = \frac{1}{4\pi d^2}\int_{E_1}^{E_2}\frac{d\dot{N}_X}{dE_X}\exp\,[-\sigma(E_X)N_H]E_X\,dE_X\,. \qquad (48)$$

In Table 3, we give the expected quantities such as temperatures (T_s, T_h, and T_h^m), the typical energy of a primary curvature photon at the inner boundary (eq. [4]), the distance from the star of the first generation of $e^\pm$ pairs (r_s/R), and the product of r_a and τ_{max} for all X-ray pulsars with an inclination angle of 60°. One can see from Table 3 that the positions of the first generation of $e^\pm$ pairs ranges from 10 to 40 stellar radii for canonical pulsars, but are close to the

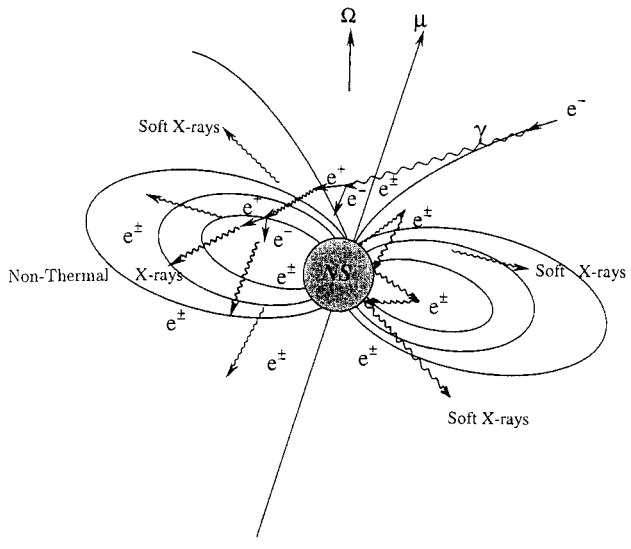

FIG. 2.—Absorption coefficient vs. the distance to the star for Geminga, PSR B1055−52, and PSR B0656+14.

star surface for millisecond pulsars. In our calculations, we found that $f > 1$ for older pulsars, PSR B1929+10, PSR B0950+08, and PSR B0823+26 (ages $10^{6.49}$, $10^{7.24}$, and $10^{6.69}$ yr, respectively), so we believe that the outer gaps do not exist in these three pulsars. In Figure 2 we show the absorption coefficient versus distance for Geminga, PSR B1055−52, and PSR B0656+14.

4. POLAR-CAP HEATING

For the X-ray emission from relatively old canonical pulsars, such as PSR B1929+10 and PSR B0950+08, for which the fractional size of the outer gap would be greater than unity in our model, the outer gaps do not exist. Because their surface temperatures are expected to be less than 10^5 K (e.g., Nomoto & Tsuruta 1987; Page & Applegate 1992), the observed X-rays from these pulsars may not come from the cooling surface. Here we consider the X-ray emission from polar-cap heating.

According to the polar-cap model proposed by RS, electrons will be stripped from the stellar surface, but the ions will be retained because of their higher surface binding energy. Therefore, the stellar surface does not supply the positive charges to replace the positive charges in the magnetosphere if $\boldsymbol{\Omega} \cdot \boldsymbol{B} < 0$, and a vacuum gap will form above the polar caps. The gap will continue to expand at a speed of $\sim c$ until it reaches a maximum height h, which corresponds to a gap potential large enough to ignite an $e^{\pm}$ cascade. The gap potential and h can be determined by the condition of pair production, which is

$$\frac{E_\gamma}{2m_e c^2}\frac{B_s h/s}{B_q} \geq \frac{1}{15} \tag{49}$$

(Erber 1966; RS). Since the electrons/positrons are accelerated in the gap, $\gamma_e = e\Delta\Phi/m_e c^2$. The gap height and potential drop are given by (RS)

$$h_{\rm RS} = 5 \times 10^3 s_6^{2/7} P^{3/7} B_{12}^{-4/7} \text{ cm} \tag{50}$$

and

$$\Delta\Phi \equiv \Delta V_{\rm RS} = 1.6 \times 10^{12} s_6^{4/7} P^{-1/7} B_{12}^{-1/7} \text{ V} . \tag{51}$$

RS suggested that when the gap potential drop reaches $\Delta V_{\rm RS}$, a spark discharge occurs inside the gap, triggering an avalanche of $e^{\pm}$ pairs, which in turn will result in the pair-production cascade envisaged by Sturrock (1971). The difference from Sturrock's model is that in the RS model the acceleration occurs only in the vacuum gap ($\boldsymbol{E} \cdot \boldsymbol{B} \neq 0$) at a height $h = h_{\rm RS} < r_{\rm pc}$. Outside the gap ($\boldsymbol{E} \cdot \boldsymbol{B} = 0$), the pairs are no longer accelerated and stream outward with a Lorentz factor of ~ 3. RS showed that the density of the streaming pairs is much higher than the Goldreich-Julian density, so the plasma will be essentially charge neutral. Furthermore, they suggested that radio emission occurs above the spark regions in the filled, streaming region where bunching by plasma instabilities would lead to coherent radio emission. It should be pointed out that the polar-cap charge density is negative when $\boldsymbol{\Omega} \cdot \boldsymbol{\mu} > 0$. Electrons with much weaker binding energy can be pulled out from the stellar surface and form a steady outflow current. Because of the finite inertia of electrons, the potential of the polar gap cannot be zero. It is shown that

$$\Delta V_s \approx \frac{\Omega^2 \mu}{c^2}\frac{R}{s} \sim 10^{11} \mu_{30} P^{-5/2} \text{ V} , \tag{52}$$

which is called the space-charge–limited potential (see Arons & Scharlemann 1979; Arons 1997 for a review). However, Muslimov & Tsygan (1992) have shown that the actual potential drop for the space-charge–limited flow is much larger than that in equation (52) if general relativistic effects are included. The corrected space-charge–limited potential should be

$$\Delta V_s \approx \frac{10R}{s}\frac{\Omega^2 \mu}{c^2}\left[1 - \left(\frac{R}{r}\right)^3\right] \sim 10^{14} \mu_{30} P^{-5/2}\left[1 - \left(\frac{R}{r}\right)^3\right] \text{ V} , \tag{53}$$

which is even larger than $\Delta V_{\rm RS}$, where μ_{30} is the magnetic moment in units of 10^{30} cgs. It is further suggested that the large potential drop may explain γ-ray emission from young pulsars (e.g., Muslimov & Harding 1997). However, equation (53) has ignored the pair production inside the gap. Unless the surface magnetic field is purely dipolar, the pair cascade should restrict the potential of the cap as shown in equation (51).

We have argued in § 3.3 that the surface magnetic field of a pulsar should in general be dominated by the strong surface local magnetic field instead of a pure dipole field. If the surface magnetic field is indeed dominated by a much stronger local field B_s, then the actual polar-cap area can be estimated from equation (28). The strong surface magnetic field and the small radius of curvature means that equation (49) no longer gives the minimum condition for pair production, i.e., $B_s \geq (B_q/15)(s/h_{\rm RS})$; instead, we have

$$E_\gamma \geq 2mc^2 \tag{54}$$

as the minimum condition for pair production. Equation (54) gives

$$h = 1.1 \times 10^2 s_5^{1/6} P^{1/2} B_*^{-1/2} \tag{55}$$

and

$$\Delta V = 7.5 \times 10^{10} s_5^{1/3} \text{ V} , \tag{56}$$

where $B_* = B_s/10^{14}$ G.

Therefore, the thermal X-ray luminosity due to polar-cap heating can be approximated as

$$L_{\rm X}^p \approx 1.7 \times 10^{29} B_{d,12} P^{-2} s_5^{1/3} \text{ ergs s}^{-1} . \tag{57}$$

Using the polar-cap area given in equation (28), the polar-cap temperature is

$$T_p = 6.2 \times 10^6 B_*^{1/4} P^{-1/4} s_5^{-1/12} \text{ K} , \tag{58}$$

where $s = l$ has been used. We will use equations (57) and (58) to explain the X-ray emission from the pulsars whose outer gaps do not exist, such as PSR B1929+10.

5. THE EFFECT OF INCLINATION ANGLE AND VIEWING ANGLE

In our model, the magnetic inclination angle plays an important role in the nonthermal X-ray emission from pulsars. In fact, if the inclination angle of a pulsar is very small, then the nonthermal X-rays may be too weak to be observed; otherwise, the nonthermal X-rays may be dominant. In addition, the viewing angle, ζ, also plays an important role in the thermal X-ray emission from a pulsar. For a

pulsar with a small inclination angle, if the viewing angle is close to the inclination angle, then we expect that soft thermal X-rays and hard thermal X-rays will be observed; otherwise, only soft thermal X-rays will be observed. Furthermore, for a pulsar with a large inclination angle, we expect the observed X-rays to consist of soft thermal, hard thermal, and nonthermal X-rays if the viewing angle is close to the inclination angle; otherwise, only soft thermal and nonthermal X-rays will be seen if $|\zeta - \chi|$ is larger than θ_h. Therefore, we expect four possible types of X-ray spectra, depending on the inclination angles and viewing angles of pulsars: (1) soft thermal X-rays, (2) the sum of soft thermal X-rays and hard thermal X-rays, (3) the sum of soft thermal and nonthermal X-rays, and (4) the sum of soft thermal, hard thermal, and nonthermal X-rays.

The inclination angles and viewing angles of some pulsars have been indirectly estimated by using radio data and/or γ-ray data. Lyne & Manchester (1988) and Rankin (1993) estimated the inclination angles and viewing angles of some pulsars using radio data. Using radio and γ-ray data and their model of γ-ray emissions from pulsars, Romani & Yadigaroglu (1995) and Yadigaroglu & Romani (1995) have estimated the inclination angles and viewing angles of γ-ray pulsars and candidates, most of which are also X-ray emitters. In Table 4, we list possible values of the inclination and viewing angles of some pulsars.

As an example, we consider the dependence of the X-ray spectrum of a pulsar with period $P = 0.2$ s and magnetic field $B_{12} = 1.5$ on various inclination angles and viewing angles, where $N_{\rm H} = 1.5 \times 10^{20}$ cm^{-2}, $\xi = 0.1$, $d = 0.4$ kpc, $B_* = 1$, and $s_5 = 1$ are assumed. We consider two cases. First, we choose a small value of the inclination angle, say $\chi = 20°$, and different values of the viewing angle ($\zeta = 60°$ and 20°). The expected spectra are shown in Figures 3*a* and 3*b*. It can be seen that there are two possible spectra, one consisting of only soft thermal X-rays, if the viewing angle is far away from the inclination angle, and the other consisting of two components (soft thermal plus hard thermal), when the viewing angle is close to the inclination angle. Finally, we choose a large value of the inclination angle ($\chi = 60°$) and different values of the viewing angle ($\zeta = 60°$ and 90°). These results are shown in Figures 3*d* and 3*c*. We expect the X-ray spectrum to consist of four components if the viewing angle is close to the inclination angle, and of only two components (of which the modulated thermal hard X-ray component is not visible) if the viewing angle is much larger than the inclination angle.

TABLE 4

POSSIBLE INCLINATION AND VIEWING ANGLES OF X-RAY PULSARS

Pulsar	χ (deg)	$\zeta - \chi$ (deg)	Reference
B0531+21.....	84	...	1
	80	−18	2
B0833−45.....	90	12	1
	65	14	2
	90	6.4	3
B0633+17.....	~40	50	2
B1706−44.....	42	25	2
B1509−58.....	60	15	2
B1823−13.....	30	...	2
J0437−47	35	5	4
B0656+14.....	30	...	1
	8	8	2
	8.2	8.2	3
B1055−52.....	90	0	1
	70	−8	2
	17.9	9.8	3
B0355+54.....	51	4.4	1
	51	4	2

REFERENCES.—(1) Rankin 1993; (2) Romani & Yadigaroglu 1995; (3) Lyne & Manchester 1988; (4) Manchester & Johnston 1995.

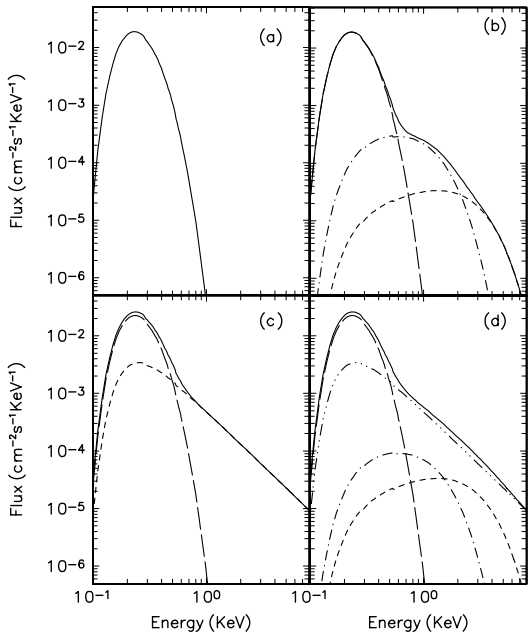

FIG. 3.—Possible X-ray spectra of the pulsar with various viewing angles (ζ) and inclination angles (χ). (*a*) $\chi = 20°$ and $\zeta = 60°$; only soft X-rays can be seen (*solid curve*). (*b*) $\chi = 20°$ and $\zeta = 20°$; the X-ray emission (*solid curve*) consists of a soft thermal X-ray component (*long-dashed curve*) and two hard X-ray components that result from polar-cap heating by the return current in the polar gap (*short-dashed curve*) and by the return current from the outer gap (*dash-dotted curve*). (*c*) $\chi = 60°$ and $\zeta = 90°$; the X-ray emission (*solid curve*) consists of soft thermal X-ray (*long-dashed curve*) and nonthermal X-ray (*short-dashed curve*) components. (*d*) $\chi = 60°$ and $\zeta = 60°$; the X-ray emission (*solid curve*) consists of a nonthermal X-ray component (*dot-dot-dashed curve*), a soft thermal X-ray component (*long-dashed curve*), and two hard X-ray components that result from polar-cap heating by the return current in the polar gap (*short-dashed curve*) and by the return current from the outer gap (*dot-dashed curve*). We have assumed that the pulsar has a period of 0.2 s and a magnetic field of 10^{12} G, and that $\xi = 0.1$.

6. THE COMPARISON OF MODEL RESULTS WITH OBSERVED DATA

6.1. *The Comparison of Expected Luminosity with Observations*

We will compare our model results with the observations of *ROSAT* (Becker & Trümper 1997) and *ASCA* (Saito et al. 1997). Cheng et al. (1998) assumed that all X-ray pulsars have nonthermal origins and compared the model results, equations (38) or (39), with *ROSAT* observations of the pulsars reviewed by Becker & Trümper (1997). They have shown that the linear relationship and scatter of $L_{\rm X}$ around $10^{-3} L_{\rm sd}$ values are well reproduced by their model and that the scatter is due to a numerical factor that depends on P and B, which should be largest for small P and B values. However, the major factor in causing scatter of the data is

the inclination angle. Therefore, they pointed out that the discrepancies between the observed and model values of L_X result from the actual value of the inclination angle, which was set to be $\chi = 55°$ in the model calculations. However, Cheng et al. (1998) did not consider the contribution of thermal X-rays. Here we will take this contribution into account in comparing model results with the *ROSAT* observations, in which we assume that the hard thermal X-rays cannot make a significant contribution to *ROSAT* observations, and $\xi = 0.1$. In Figure 4, we show a comparison of model results with the observed X-ray luminosities of the pulsars seen by *ROSAT* (the energy range is from 0.1 to 2.4 keV), where the inclination angle is assumed to be 60°. We did not include three older pulsars, PSR B1929+10, PSR B0950+08, and PSR B0823+26, because their outer-gap sizes are greater than unity in our model. It can be seen from Figure 4 that our model can reproduce the linear relationship of L_X around $10^{-3}L_{sd}$, and that the scatter is due to the numerical factor depending on P, B_{12}, and the inclination angle. It should be noted that the contribution of the nonthermal X-rays emitted directly from the outer gap is negligible for Vela-like pulsars (Cheng et al. 1986b; Zhang & Cheng 1997). On the other hand, the outer-gap X-rays dominate all other X-ray components for Crab-like pulsars.

In Figure 5, we also compare our model results with X-ray luminosities of the pulsars observed by *ASCA* (the energy range of X-rays is from 2 to 10 keV), where the inclination angle is set to 60°. One can see from Figure 5 that both the linear relationship and scatter of L_X around $\sim 2.5 \times 10^{-9} L_{sd}^{1.15}$ are produced by our model, which differs from the observed $L_X \approx L_{sd}^{1.5}$ (Saito et al. 1997). From the theoretical point of view, the discrepancies between the observed and model values of L_X could possibly result from (1) the actual value of the inclination angle and viewing angle and/or (2) ignoring the contribution of the non-

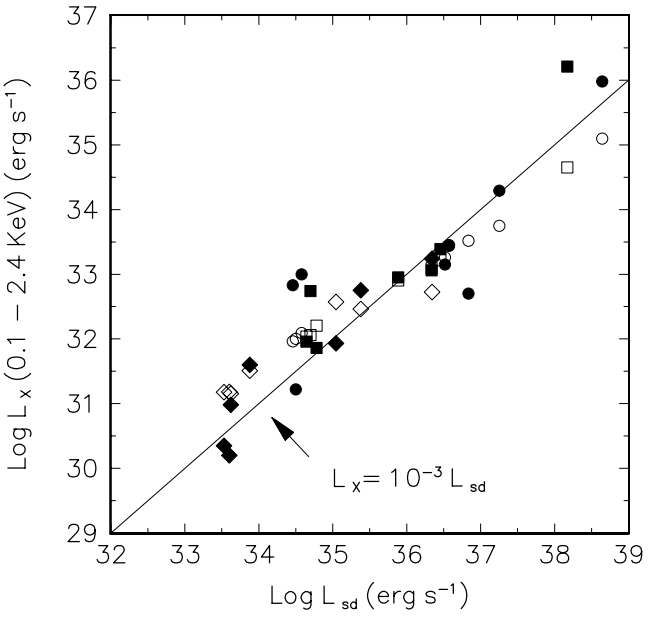

FIG. 4.—Plot of the X-ray pulsar luminosity vs. spin-down luminosity for 22 pulsars. The *ROSAT* data (0.1–2.4 keV) are taken from Becker & Trümper (1997). Data points for eight γ-ray pulsars, seven radio pulsars, and seven millisecond pulsars are represented by filled circles, boxes, and diamonds, respectively; theoretical values are represented by open symbols.

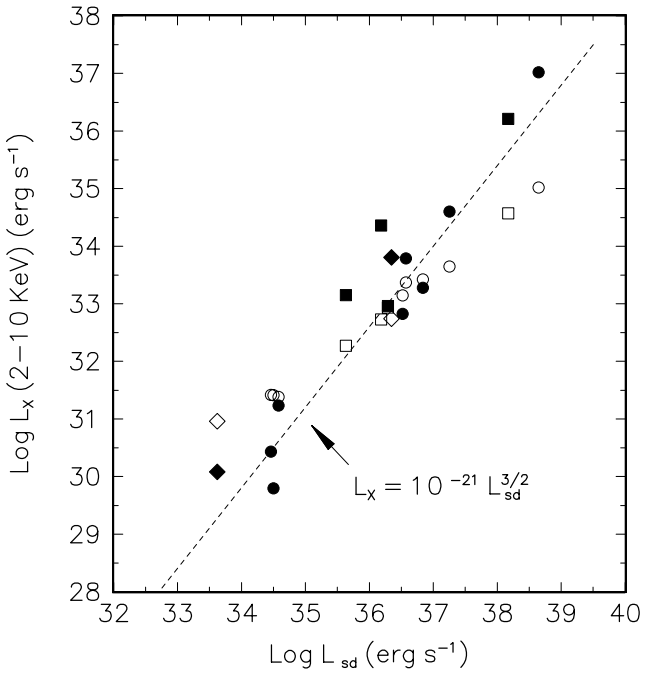

FIG. 5.—Plot of the pulsed X-ray luminosity vs. spin-down luminosity for 14 pulsars. The *ASCA* data (2–10 keV) are taken from Saito et al. (1997). Data points from eight γ-ray pulsars, four radio pulsars, and two millisecond pulsars are represented by filled circles, boxes, and diamonds, respectively; theoretical values are represented by open symbols.

thermal X-rays directly emitted from the outer gap for the Crab-like pulsars (cf. Cheng et al. 1986b). In fact, in the *ASCA* energy range, the main contribution in our model comes from the nonthermal X-rays, a component that depends strongly on the inclination angles of the pulsars. Although the actual inclination angles of most pulsars are not yet known, some of them have been indirectly derived (see Table 4). For example, our model predicts that the X-ray luminosity is $\sim 10^{36.9}$ ergs s^{-1} for the Crab, with $\chi = 75°$; $\sim 10^{33.5}$ ergs s^{-1} for Vela, with $\chi = 64°$; and $\sim 10^{30.1}$ ergs s^{-1} for Geminga, with $\chi = 52°$.

6.2. *The X-Ray Spectra from Geminga and PSR B1055−52*

Now we compare our model results with the X-ray data for the Geminga and PSR B1055−52 pulsars. The Geminga pulsar has a period of 0.237 s, surface magnetic field of $\sim 1.6 \times 10^{12}$ G, and characteristic age of 3.4×10^5 yr. PSR B1055−52 is a Geminga-like pulsar with a period of 0.197 s, surface magnetic field 10^{12} G, and a characteristic age of $\sim 5.3 \times 10^5$ yr. Although they have the same basic features, such as period, spin-down power, characteristic age, etc., their observed X-ray luminosities (see Table 1) and spectra (see Figs. 6 and 7) are very different. We try to explain these differences in this section.

Halpern & Ruderman (1993) studied the X-rays from Geminga using the *ROSAT* observations and fitted the observed spectrum with a two-component model, either two blackbodies or a blackbody plus a power law. Halpern & Wang (1997) presented a comprehensive study of the Geminga pulsar at energies of 0.1–10 keV using *ASCA*, *ROSAT*, and *EUVE* observations. They fitted the X-ray spectrum of Geminga with a blackbody plus a power law. Their fitting results indicate that (1) the soft X-ray component is from a blackbody with a temperature of $\sim 5.8 \times 10^5$ K and a bolometric luminosity of 1.47×10^{31}

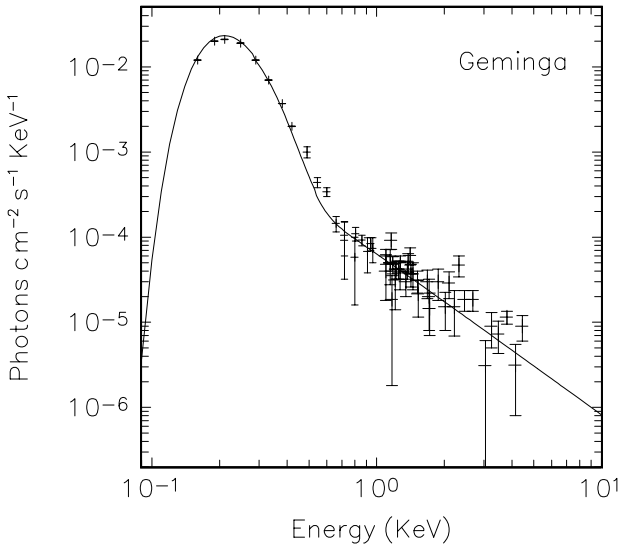

FIG. 6.—Comparison of model results with the *ASCA* and *ROSAT* data for Geminga. The observed data are taken from Halpern & Wang (1997).

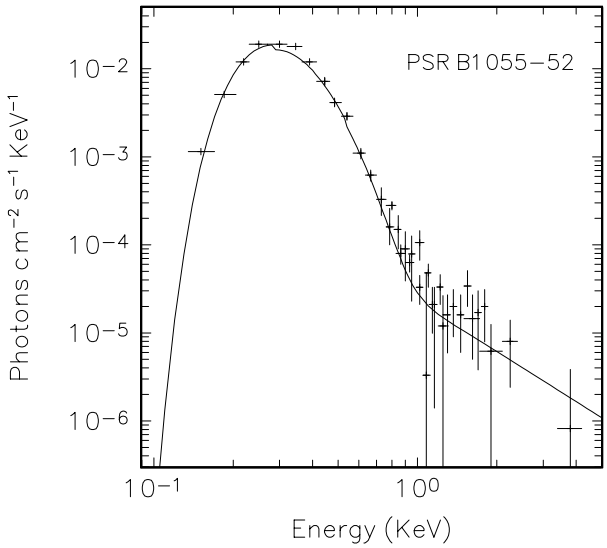

FIG. 7.—Comparison of model results with the *ASCA* and *ROSAT* data for PSR B1055−52. The observed data are taken from Wang et al. (1998).

ergs s^{-1}, and (2) the hard X-ray component is fitted by a power law with spectral index $\sim 1.5 \pm 0.2$ and a luminosity of 8.13×10^{29} ergs s^{-1}. Furthermore, Geminga is believed to be a radio-quiet pulsar; the viewing angle is larger than the inclination angle (e.g., Romani & Yadigaroglu 1995), so the hard thermal X-rays cannot be observed. In Figure 6, we show a comparison of our model results with the observed data, where $\chi \approx 50°$ and interstellar absorption has been taken into account assuming $N_{\rm H} = 1.5 \times 10^{20}$ cm^{-2}.

The X-ray spectrum of PSR B1055−52 has also been fitted with a two-component model (Ögelman & Finley 1993; Greiveldinger et al. 1996; Possenti et al. 1996; Wang et al. 1998). The soft X-ray component is fitted by a blackbody with a temperature of $\sim 7.9 \times 10^5$ K, and the hard X-ray component is fitted by a power law with a spectral index of $\sim 1.5 \pm 0.3$ (Wang et al. 1998). We show the comparison of our model results with the observed data in Figure 7, where $\chi \approx 52°$ and interstellar absorption has been taken into account assuming $N_{\rm H} = 2.6 \times 10^{20}$ cm^{-2}.

6.3. *The X-Ray Spectrum from PSR B0656+14*

Although PSR B0656+14 has many similarities with Geminga and PSR B1055−52, γ-ray emission from it has not yet been confirmed completely (Ramanamurthy et al. 1996). X-ray emission from PSR B0656+14 has been observed by *ROSAT* and *ASCA* (e.g., Ögelman 1995; Possenti et al. 1996; Greiveldinger et al. 1996; Becker & Trümper 1997; Wang et al. 1998). Greiveldinger et al. (1996) suggested that the X-ray spectrum can be fitted by two blackbodies and a power law, while Wang et al. (1998) pointed out that it can be fitted by the double blackbody model but failed to confirm the extra power-law component. According to Wang et al. (1998), the soft X-ray component has a temperature of $\sim 8.1 \times 10^5$ K and bolometric luminosity of 4.3×10^{32} ergs s^{-1}; the hard X-rays have a temperature of $\sim 1.7 \times 10^6$ K and a bolometric luminosity of 2.6×10^{31} ergs s^{-1} (where the distance to this pulsar is 400 pc). It is very important to note that from the observed temperature and luminosity of the hotter component, the area that produces the hard X-rays is larger than the canonical polar-cap area, $A_{p0} = \pi R^2(\Omega R/c)$, by a factor of 15–30 (Greiveldinger et al. 1996; Wang et al. 1998). We argue that the actual polar-cap area will be larger than that of a pure dipole field because of the much stronger components of magnetic field near the polar cap of PSR B0656+14 (see eq. [31]).

Furthermore, by analyzing the observed modulation, Possenti et al. (1996) suggested that the inclination angle of this pulsar is $\sim 30°$, which is the same as that given by Rankin (1993). If the inclination angle is $\sim 30°$, then the contribution of the nonthermal X-rays to the total X-rays from PSR B0656+14 in our model is small. Since the γ-ray emission from PSR B0656+14 is much weaker than that predicted by the outer-gap model, it is suggested that the viewing angle must be $0° \leq \zeta \leq 45°$ (Romani & Yadigaroglu 1995). It is reasonable to assume that the viewing angle is close to the inclination angle, so that the soft thermal and hard thermal X-rays from PSR B0656+14 will be observed, but the nonthermal component, which is weak in our model, will not. The distance to this pulsar is uncertain. From the radio dispersion measure, it is estimated that the distance is about 760 pc (Taylor, Manchester, & Lyne 1993); from analysis of X-ray observations, it is not larger than 250 pc (Finley, Ögelman, & Kiziloglu 1992). Recently, based on the *Hubble Space Telescope* (*HST*) observations, Pavlov, Welty, & Cordova (1997) estimated that the distance is about 280 pc. Here we assume $d = 280$ pc, $\chi = 30°$. Comparing model results with the observed luminosity, we deduce that most hard thermal X-rays are reflected; only about 5% of the hard thermal X-rays escape from the open field lines, which is very consistent with equation (25). Figure 8 shows a comparison of our model results with the observed data, where $N_{\rm H} = 1.9 \times 10^{19}$ cm^{-2}; the solid curve represents model results for the inclination angle of 30°. We find that the model results for the inclination angle of $\sim 47°$ can also fit the observed data, especially for the higher energy data (see Fig. 8, *dashed curve*).

6.4. *The X-Ray Emission from PSR B1929+10*

PSR B1929+10 is a relatively old pulsar, with typical age of $\sim 10^7$ yr. The X-ray emission from this pulsar has been

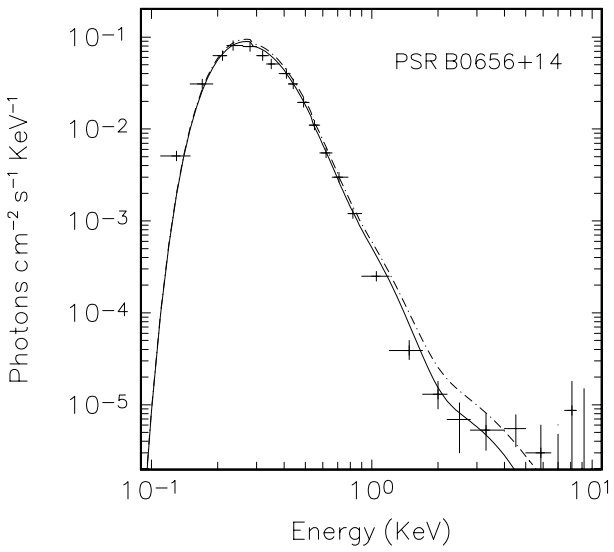

FIG. 8.—Comparison of model results with the *ASCA* and *ROSAT* data for PSR B0656+14. The observed data are taken from Greiveldinger et al. (1996).

detected by both *ROSAT* (Yancopoulos, Hamilton, & Helfand 1994; Manning & Willmore 1994) and *ASCA* (Wang & Halpern 1997). The X-ray luminosity is 1.54×10^{30} ergs s^{-1} when a distance of 250 pc is used, and the X-ray spectrum from this pulsar can be fitted by a single blackbody spectrum with a temperature of $(5.14 \pm 0.53) \times 10^6$ K from a small area (Wang & Halpern 1997). Wang & Halpern (1997) suggested that PSR B1929+10 indicates that its polar-cap area is 2 orders of magnitude less than A_d, which is calculated by assuming a dipole field structure. If the observed polar-cap areas for PSR B1929+10 indeed result from the surface multipole field, this implies $B_m \sim 10^{14}$ G (cf. eq. [28]). Such a strong multipole field could be localized in a region with a linear dimension of $l \sim (A_p^m)^{1/2} \leq 10^5$ cm, which implies that the local radius of curvature $s \sim l$. Using equations (57) and (58), $B_* = 0.1$, and $s \sim 10^5$ cm, we obtain $L_X^p \sim 1.7 \times 10^{30}$ ergs s^{-1} and $T_p \sim 5.1 \times 10^6$ K for PSR B1929+10, which is consistent with the observations.

7. DISCUSSION

We have presented a model of X-ray emission from rotation-powered pulsars. For the pulsars with outer gaps, the X-ray emission consists of two components, thermal and nonthermal. As a result of the collision of return particles from the outer gap onto the stellar surface (polar caps), hard thermal X-rays are produced. Some of the hard thermal X-rays will be effectively reflected back to the stellar surface through cyclotron resonance scattering, and eventually be reemitted as soft thermal X-rays. Furthermore, some of the hard thermal X-rays can escape along the open magnetic field lines, so they are modulated. If a strong surface magnetic field exists near the stellar surface, then a cascade should develop, and the area over which $e^{\pm}$ pairs collide with the stellar surface will be greater than the polar-cap area $A_{\rm cap}$ and will result in a decrease of the hard thermal X-ray temperature, while the soft thermal X-ray temperature does not change. Nonthermal X-rays come from synchrotron radiation of $e^{\pm}$ pairs created in the strong pulsar magnetic field near the neutron star surface by curvature photons emitted by charged particles on their way from the outer gap to the neutron star surface. Our model indicates that there are four possible X-ray spectra, depending on the magnetic inclination angle and viewing angle: soft thermal, soft thermal plus hard thermal, soft thermal plus hard thermal plus nonthermal, and soft thermal plus nonthermal (see Fig. 3). For the pulsars without outer gaps, such as PSR B0950+08 and PSR B1929+10, X-ray emission is thermal and is produced by polar-cap heating (see § 5). Using the expected X-ray luminosity in our model, we show a comparison of model results with the observed luminosities of 25 X-ray pulsars seen by *ROSAT* and *ASCA* respectively (see Figs. 4 and 5). We also apply our model to explain the observed X-ray spectra from Geminga, PSR B1055−52, and PSR B0656+14.

We would like to point out that we have ignored the thermal X-rays from neutron star cooling. In fact, the thermal X-ray flux from cooling is anisotropic, beamed mostly along the local magnetic field (e.g., Pavlov et al. 1994), which will affect the fraction of thermal X-rays among the X-rays from the polar cap escaping directly along the poles and also modulate the soft thermal component, even though the entire surface is emitting.

The relative phases of different X-ray components in our model are not easily determined. In principle, the two hard thermal X-ray components come from the stellar surface; they should peak at the same phase. The hard nonthermal X-ray component should peak at the plane of (Ω, μ), where the outer gap is located. But the relative phase between the hard thermal X-rays and the hard nonthermal X-rays could be different, because of aberration effects and the different locations of the dipolar and multipolar axes. The relative phase between thermal hard X-rays and thermal soft X-rays should be of the order of 180°, plus the correction due to the position difference between the dipolar and multipolar axes.

Finally, the nonthermal hard X-rays from the outer gap in Crab-type pulsars can be greater than that given here.

We thank the anonymous referee for his/her constructive comments and P. K. Mackeown for proofreading our manuscript. This work is partially supported by a RGC grant from the Hong Kong Government.

REFERENCES

Alpar, M. A., Anderson, P. W., Pines, D., & Shaham, J. 1984, ApJ, 278, 791
Arons, J. 1981, ApJ, 248, 1099
———. 1993, ApJ, 408, 160
———. 1997, in Neutron Stars and Pulsars: Thirty Years after Discovery, ed. N. Shibazakiet et al. (Tokyo: Universal Academy Press), 339
Arons, J., & Scharlemann, E. T. 1979, ApJ, 231, 854
Arons, J., & Tavani, M. 1993, ApJ, 403, 249
Becker, W., & Trümper, J. 1997, A&A, 326, 682
Blandford, R. D., Applegate, J. H., & Hernquist, L. 1983, MNRAS, 204, 1025
Cheng, K. S. 1987, ApJ, 321, 805
Cheng, K. S., Chau, W. Y., Zhang, J. L., & Chau, H. F. 1992, ApJ, 396, 135
Cheng, K. S., Gil, J., & Zhang, L. 1998, ApJ, 493, L35
Cheng, K. S., Ho, C., & Ruderman, M. A. 1986a, ApJ, 300, 500
———. 1986b, ApJ, 300, 522
Cheng, K. S., & Zhang, J. L. 1996, ApJ, 463, 271
Edelstein, J., Foster, R. S., & Bowyer, S. 1995, ApJ, 454, 442
Erber, T. 1966, Rev. Mod. Phys., 38, 626
Finley, J., Ögleman, H., & Kiziloglu, U. 1992, ApJ, 394, L21
Freese, K., Turner, M., & Schramm, D. N. 1983, Phys. Rev. Lett., 51, 1625
Gil, J., & Cheng, K. S. 1998, in preparation
Goldreich, P., & Julian, W. H. 1969, ApJ, 157, 869
Greiveldinger, C., et al. 1996, ApJ, 465, L35
Halpern, J. P., & Ruderman, M. A. 1993, ApJ, 415, 286

Halpern, J. P., & Wang, F. Y.-H. 1997, ApJ, 477, 905
Harding, A. K., Ozernoy, L. M., & Usov, V. V. 1993, MNRAS, 265, 921
Lyne, A. G., & Manchester, R. N. 1988, MNRAS, 234, 477
Manchester, R. N., & Johnston, S. 1995, ApJ, 441, 65
Manning, R. A., & Willmore, A. P. 1994, MNRAS, 266, 635
Morrison, R., & McCammon, D. 1983, ApJ, 270, 119
Muslimov, A. G., & Harding, A. K. 1997, ApJ, 485, 735
Muslimov, A. G., & Tsygan, A. I. 1992, MNRAS, 255, 61
Nel, H. I., et al. 1996, ApJ, 465, 898
Nomoto, K., & Tsuruta, S. 1987, ApJ, 312, 711
Ögelman, H. 1995, in Lives of Neutron Stars, ed. A. Alpar, U. Kilizoglu, & J. Van Paradijs (Dordrecht: Kluwer), 101
Ögelman, H., & Finley, J. P. 1993, ApJ, 413, 310
Paczyski, B. 1990, ApJ, 348, 485
Page, D., & Applegate, J. H. 1992, ApJ, 394, 17
Pavlov, G. G., Shibanov, Yu. A., Ventura, J., & Zavlin, V. E. 1994, A&A, 289, 837
Pavlov, G. G., Welty, A. D., & Cordova, F. A. 1997, ApJ, 489, L75
Possenti, A., Mereghetti, S., & Colpi, M. 1996, A&A, 313, 565
Ramanamurthy, P. V., et al. 1996, ApJ, 458, 755
Rankin, J. M. 1993, ApJ, 405, 285
Romani, R. W. 1990, Nature, 347, 741
Romani, R. W., & Yadigaroglu, I. 1995, ApJ, 438, 314
Ruderman, M. A. 1991a, ApJ, 366, 261
———. 1991b, ApJ, 382, 576
———. 1991c, ApJ, 382, 587
Ruderman, M. A., & Sutherland, P. 1975, ApJ, 196, 57 (RS)
Saito, Y., Kawai, N., Kamae, T., & Shibata, S. 1997, in Neutron Stars and Pulsars: Thirty Years after Discovery, ed. N. Shibazaki et al. (Tokyo: Universal Academy Press), 295
Shibazaki, N., & Lamb, F. 1989, ApJ, 346, 808
Sturrock, P. A. 1971, ApJ, 164, 529
Taylor, J. H., Manchester, R. N., & Lyne, A. G. 1993, ApJS, 88, 529
Thompson, D. J., et al. 1996, ApJS, 107, 227
Wang, F. Y.-H., & Halpern, J. P. 1997, ApJ, 482, L159
Wang, F. Y.-H., Ruderman, M., Halpern, J. P., & Zhu, T. 1998, ApJ, 498, 373
Yadigaroglu, I., & Romani, R. W. 1995, ApJ, 446, 543
Yancopoulos, S., Hamilton, T. T., & Helfand, D. J. 1994, ApJ, 429, 832
Zhang, L., & Cheng, K. S. 1997, ApJ, 487, 370